JCTC Journal of Chemical Theory and Computation

Time-Dependent Properties of Liquid Water: A Comparison of Car−Parrinello and Born−Oppenheimer Molecular Dynamics Simulations

I-Feng W. Kuo,[†] Christopher J. Mundy,[†] Matthew J. McGrath,[‡] and J. Ilja Siepmann*[,‡]

Chemistry and Materials Science Directorate, Lawrence Livermore National Laboratory, Livermore, California 94550, and Departments of Chemistry and of Chemical Engineering and Material Science, University of Minnesota, 207 Pleasant Street SE, Minneapolis, Minnesota 55455-0431

Received June 5, 2006

Abstract: A series of 30 ps first principles molecular dynamics simulations in the microcanonical ensemble were carried out to investigate transport and vibrational properties of liquid water. To allow for sufficient sampling, the thermodynamic constraints were set to an elevated temperature of around 423 K and a density of 0.71 g cm^{-3} corresponding to the saturated liquid density for the Becke−Lee−Yang−Parr (BLYP) representation of water. Four simulations using the Car−Parrinello molecular dynamics (CPMD) technique with varying values of the fictitious electronic mass (μ) and two simulations using the Born−Oppenheimer molecular dynamics (BOMD) technique are analyzed to yield structural and dynamical information. At the selected state point, the simulations are found to exhibit nonglassy dynamics and yield consistent results for the liquid structure and the self-diffusion coefficient, although the statistical uncertainties in the latter quantity are quite large. Consequently, it can be said that the CPMD and BOMD methods produce equivalent results for these properties on the time scales reported here. However, it was found that the choice of μ affects the frequency spectrum of the intramolecular modes, shifting them slightly to regions of lower frequency. Using a value of $\mu = 400$ au results in a significant drift in the electronic kinetic energy of the system over the course of 30 ps and a downward drift in the ionic temperature. Therefore, for long trajectories at elevated temperatures, lower values of this parameter are recommended for CPMD simulations of water.

Introduction

Water's ubiquity on Earth leads to a vital role in most biological and environmental processes, either directly or indirectly. As a result, water has been studied by experimental, theoretical, and computational methods for many years. However, water deviates in many important ways from simple fluids to the extent of becoming a grand challenge for both liquid state theory and molecular simulation.[1,2] Originally, particle-based simulations employed empirical potentials for the determination of energies and forces,[3] but some of water's physical (e.g. a large dipole moment and large polarizability) and chemical (such as self-dissociation) properties have made it difficult to use an empirical force field to accurately reproduce experimental data over a wide range of state points.

The advent of the Car−Parrinello (CP) method in 1985[4] enabled one to use a quantum mechanical description of the electronic degrees of freedom combined with a classical phase space trajectory involving a fictitious electronic mass parameter. The first CP molecular dynamics simulation for liquid water followed in 1993,[5] a significant advance despite that computational resources limited this simulation to 32 molecules and less than 4 ps for the combined equilibration and production periods. Since then, the increase in available

* Corresponding author e-mail: siepmann@chem.umn.edu.
[†] Lawrence Livermore National Laboratory.
[‡] University of Minnesota.

10.1021/ct6001913 CCC: $33.50
Published on Web 07/27/2006

computing power and the refinement of algorithms has led to an increased ability to perform these simulations, and the CP method has now been applied to many aqueous systems at a variety of conditions (for examples, see refs 6−10). The information obtained from these studies has substantially advanced our understanding of the physical and chemical properties of aqueous systems.

Recently, the first principles simulation protocols employed in studies of liquid water have been examined critically.[11−15] It has been suggested that the appropriate selection of the fictitious electronic mass parameter will result in consistent structural properties.[12−14] The effect of the fictitious electronic mass on dynamical properties (such as diffusion constant and vibrational frequencies) has been examined for both crystalline systems[16,17] and liquid water,[13] but a comprehensive comparison between Born−Oppenheimer (BO) and CP molecular dynamics for time-dependent properties of liquid water has been lacking. Although there is clear evidence that vibrational properties are affected by the fictitious mass parameter, it is not certain whether transport properties are sensitive to this parameter as long as reasonable values are used (which may or may not coincide with the upper range suggested by previous works for consistent structural properties). It is the goal of this study to explore this issue more thoroughly by using a range of fictitious mass parameters for CP molecular dynamics simulations and comparing the results to BO simulations that quench the electronic density at every step to a given tolerance.

The main thermophysical quantity in question is the self-diffusion coefficient. To precisely compute this quantity the molecules must move a significant distance from their starting positions, i.e., many molecular diameters. This can be achieved by increasing the simulation length, increasing the average velocity of the molecules (i.e. raising the temperature), or lowering the barrier for diffusive transport (i.e. lowering the density). Given the expense of ab initio simulations, the nuclear kinetic temperature of this study was raised to 423 K, and the density was set to the saturated liquid density for water calculated previously[18] for the Becke−Lee−Yang−Parr (BLYP) exchange and correlation functionals.[19,20] This enabled the molecules in the simulation to move on average between four and five molecular diameters from their origin for each 30 ps trajectory. A rigorous statistical analysis is presented in an attempt to determine the nature and magnitude of inconsistencies for both dynamical and structural properties, which leads to the conclusion that not all dynamical properties are affected equally by the change in fictitious electronic mass.

Simulation Methods and Details

A series of six ab initio molecular dynamics (MD) simulations was performed using the publicly available software suite CPMD.[21] Four of these simulations were based on the extended Lagrangian approach developed by Car and Parrinello.[4] The CP approach introduces a fictitious electronic kinetic energy term into the Lagrangian to efficiently propagate the electronic density (i.e. it makes the integration schemes used feasible). This allows one to use density functional theory to provide a quantum mechanical description of the electronic component of the system. In this work, the Kohn−Sham formulation of density functional theory[22] is used with the gradient corrected exchange functional of Becke[19] and the Lee−Yang−Parr correlation functional.[20] The choice of these functionals as well as the norm-conserving Martins−Troullier pseudopotentials[23] with Kleinman−Bylander transformation to the fully nonlocal form[24] to describe the core electronic states and a plane wave cutoff of 85 Ry for the Kohn−Sham orbitals follow those used in previous CPMD simulations.[14,25,26]

The use of the CP method implies that a value of the fictitious electronic mass parameter must be selected. For previous simulations of liquid water near ambient conditions and a duration of 20 ps or less, a value of $\mu = 400$ au appears to be a reasonable choice.[12,14] The goal of this work is to examine the effect of this parameter on dynamic properties of water, and, therefore, three additional choices of the fictitious mass ($\mu = 100$, 200, and 300 au) were explored. All runs using the Car−Parrinello method are labeled CP-μ. The CPMD program is also capable of quenching the electronic density after every time step instead of propagating it with the CP method. This leads to direct sampling from the Born−Oppenheimer surface. Two simulations were run using this method (quenching the energy to 10^{-7} Hartrees) in order to provide another level of comparison. These runs are labeled BO-1 and BO-2.

The initial configurations for all simulations except BO-2 were taken from the saturated liquid phase of an equilibrated Monte Carlo simulation at $T = 423$ K in the Gibbs ensemble and scaled to the computed average density of $\rho = 0.71$ g cm^{-3},[18] which corresponds to a supercell of $L = 13.9176$ Å for 64 water molecules. BO-2 was started from a configuration taken from the middle of BO-1 and rescaling the velocities to generate a slightly higher temperature. An equilibration period of about 5 ps in the canonical (*NVT*) ensemble was used to equilibrate each system and provide a random initial velocity distribution to ensure divergence of trajectories. Subsequently, production periods were run in the microcanonical (*NVE*) ensemble for 30 ps over which all reported properties were computed (unless otherwise stated). The time steps vary between runs (from 0.0484 to 0.484 fs) and are reported in Table 1.

Results and Discussion

It is well-known that all simulations utilizing the CP method suffer from some degree of nonadiabaticity between the nuclear and electronic degrees of freedom,[4,16,17,27] which is an effect that grows with increasing values of the fictitious electronic mass. This adiabaticity breakdown results in CP forces on the ions becoming significantly different than the BO forces, which necessarily impacts the trajectory. [16,17,27] More quantitative results for the system of interest (water) are shown in refs 12 and 14. In particular, ref 14 shows a simulation in the microcanonical ensemble of 64 molecules and $\mu = 800$ au being terminated after 4.4 ps due to the kinetic energy of the fictitious electronic degrees of freedom drifting by around 0.05 au. This is accompanied by an ionic temperature drop of around 30 K, which clearly demonstrates

Table 1. Simulation Details (Fictitious Mass and Time Step) and Selected Results (Average Nuclear Kinetic Temperature, Height of the First Peak in the Oxygen−Oxygen Radial Distribution Function and Diffusion Coefficient) for the Car−Parrinello (CP) and Born−Oppenheimer (BO) Molecular Dynamics Simulations[a]

run	μ (au)	δt (fs)	T_{nuc} (K)	$g_{OO}(r_{max})$	$D_{2,7}$[b] (10^{-5} cm^2 s^{-1})	$D_{7,27}$[b] (10^{-5} cm^2 s^{-1})
BO-1		0.484	417(5)	2.37(0.06)	8.3(2.7)	8.0
BO-2		0.484	426(5)	2.28(0.12)	12.4(6.5)	12.3
CP-100	100	0.048	428(7)	2.20(0.15)	12.8(5.4)	12.7
CP-200	200	0.048	422(6)	2.20(0.10)	12.3(6.6)	9.9
CP-300	300	0.073	418(10)	2.14(0.04)	12.5(3.3)	14.0
BO−SGGG[c]		0.24	393(n/a)	3.10(n/a)	1.2(n/a)	
CP−SGGG[c]	340	0.07	399(n/a)	2.60(n/a)	2.2(n/a)	

[a] The values reported are the averages of three 10 ps blocks, with the numbers in parentheses being the 95% confidence interval assuming a normal distribution. [b] $D_{2,7}$ and $D_{7,27}$ denote diffusion coefficients calculated for the 2−7 ps region of the three blocks and for the 7 to 27 ps region of the full production period, respectively. [c] CP-SGGG and BO-SGGG are simulations for the PBE functional carried out by Schwegler et al.[13]

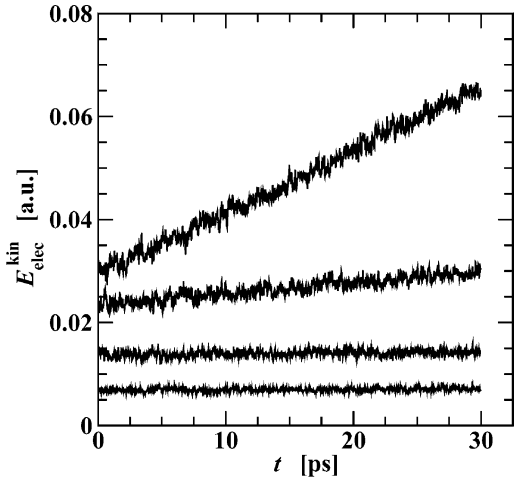

Figure 1. The instantaneous fictitious electronic kinetic energy as a function of time for all four Car−Parrinello molecular dynamics simulations. From top to bottom: CP-400, CP-300, CP-200, and CP-100.

the nonadiabaticity of the system. Figure 1 shows the electronic kinetic energy of all four CP simulations reported here as a function of time. It should be noted that one of the reported simulations (CP-400, with $\mu = 400$ au) shows a drift over the full 30 ps that is comparable to the drift for the 4.4 ps trajectory with $\mu = 800$ au from ref 14. Consequently, using a fictitious electronic mass of 400 au for long simulations of water at elevated temperature in the microcanonical ensemble cannot be recommended, and no results are shown for this run. It has been shown previously that control of the electronic degree of freedom through the use of thermostats can prevent drifting of the fictitious electronic kinetic energy,[14,28] but caution needs to be applied to remove spurious thermostating effects from dynamic properties.

Table 1 gives a summary of structural and transport properties computed for the current simulations. Errors are estimated by breaking the full trajectories into three blocks

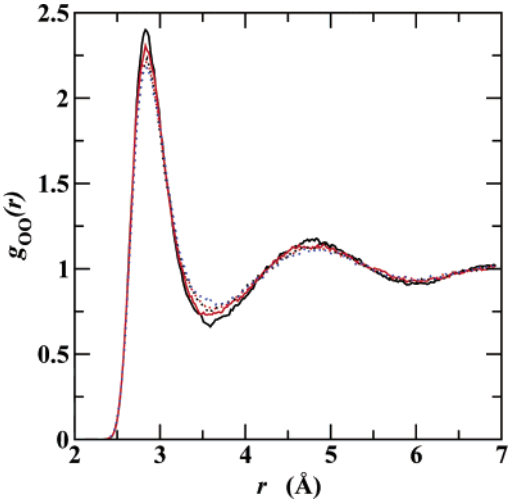

Figure 2. The oxygen−oxygen radial distribution functions obtained from molecular dynamics simulation of water using the BLYP exchange/correlation energy functional at $T = 423$ K and $\rho = 0.71$ g cm^{-3}. The lines correspond to (refer to text for descriptions) the following: BO-1 (black, solid), BO-2 (red, solid), CP-100 (black, dot), CP-200 (red, dot), and CP-300 (blue, dot).

of equal length (i.e. 10 ps), computing the property of interest, and calculating the 95% confidence interval assuming a normal distribution. Additional analysis (see below) indicates that the resulting block length of 10 ps is shorter than the correlation time for the system, and consequently the confidence intervals reported in Table 1 are probably underestimated. It can be seen from this table that the average nuclear kinetic temperatures range from 417 K (for BO-1) to 428 K (for CP-100). Despite this, the structural properties are fairly consistent, showing a spread in the first peak height of the oxygen−oxygen radial distribution function of 0.23, which is reasonable when compared to previous studies.[11−14] However, it should be noted that the 95% confidence limits for BO-1 and CP-300 do not overlap; presumably because these error limits are most likely underestimated (see below). Another possible explanation might be some type of systematic fictitious mass effect, e.g., as discussed recently by Tangney.[17]

The oxygen−oxygen and oxygen−hydrogen radial distribution functions are depicted in Figures 2 and 3. Again, agreement between the five simulations is quite good but with the (low-temperature) BO-1 simulation showing slightly more structural ordering. In comparison to other first principles simulations of liquid water, we note that simulations of supercritical water[29,30] carried out at a similar density (≈0.7 g cm^{-3}) and much higher temperatures (653 K) lead to water with significantly less structure than observed here and that simulations of dense water[13] ($\rho = 1.0$ g cm^{-3}) at elevated temperature (≈400 K) yield significantly more structure.

To compare transport properties, the self-diffusion coefficient was computed from the Einstein relation

$$2tD = \frac{1}{3}\langle|\mathbf{r}(t) - \mathbf{r}(0)|^2\rangle \quad (1)$$

where the slope is found from a linear least-squares analysis

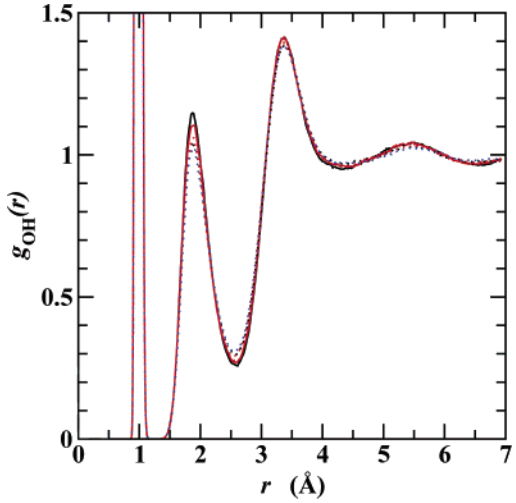

Figure 3. The oxygen−hydrogen radial distribution functions obtained from molecular dynamics simulation of water using the BLYP exchange/correlation energy functional at $T = 423$ K and $\rho = 0.71$ g cm^{-3}. The line styles and colors are the same as Figure 2.

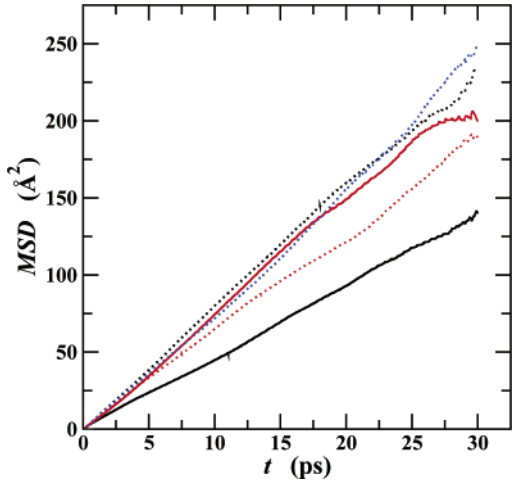

Figure 4. The mean squared displacements obtained from molecular dynamics simulation of water using the BLYP exchange/correlation energy functional at $T = 423$ K and $\rho = 0.71$ g cm^{-3}. The line styles and colors are the same as Figure 2.

to fit the 2.0−7.0 ps region of the mean square displacement (MSD). To improve statistics, origins were taken every 0.5 ps, i.e., seven time origins are used for each of the 10 ps blocks. The self-diffusion coefficients for all five simulations show overlapping confidence limits and range from 8.3 (for BO-1) to 12.8 $\times$ 10^{-5} cm^2 s^{-1} (for CP-100), suggesting that reasonable values of μ with regards to structural properties also produce consistent diffusion coefficients. A comparison of the MSD for the five simulations (see Figure 4) shows graphically the large but statistically insignificant deviations between the five simulations. In addition, we have also computed the diffusion coefficient from a least-squares analysis fit to the 7−27 ps region of the full production period. The results obtained for this longer time interval agree with the 10 ps block averages to within statistical uncertainties (see Table 1).

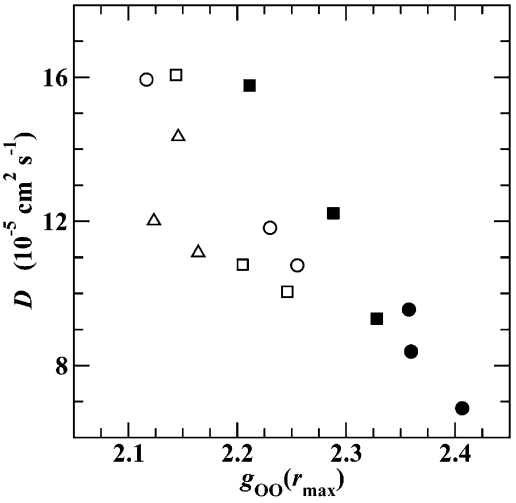

Figure 5. The diffusion coefficient as a function of the peak height of the first maximum in the oxygen−oxygen radial distribution function. Data points were obtained by dividing the simulations into three parts of equal length and computing the values for these segments. The runs are as follows: BO-1 (solid circle), BO-2 (solid square), CP-100 (open circle), CP-200 (open square), and CP-300 (open triangle up).

Assuming that the experimental correlation of high-temperature self-diffusion coefficients given in eq 4 of ref 31 can be extended to the state point investigated here (which would be inside the two-phase loop for real water), one obtains a self-diffusion coefficient of 31.8 $\times$ 10^{-5} cm^2 s^{-1}, which is approximately a factor of 3 higher than the values observed here. Thus, the BLYP representation appears to yield a liquid phase with sluggish diffusive properties, whereas it yields a vapor−liquid coexistence curve that is shifted downward.[18]

Experimentally, the self-diffusion coefficient of water changes by almost a factor of 2 for a temperature change of 20 K at lower temperatures,[32] and consequently the varying temperatures present in microcanonical simulations should be considered when comparing diffusion properties. The spread of temperatures reported here is 11 K, but there does not appear to be any strong relation between the temperature and diffusion coefficient, suggesting that other factors may influence the simulation more. For instance, one must consider how the transient changes in structure affect diffusion. Movement in a more structured fluid results in a higher barrier for diffusive transport (escape from the surrounding solvation shell), which in turn produces a slower self-diffusion coefficient. Figure 5 shows a plot of the self-diffusion coefficient as a function of the height of the first peak in the oxygen−oxygen radial distribution function for all 15 10-ps blocks used in the statistical analysis in Table 1. Using an unweighted least-squares method to fit a straight line to these points gives a correlation coefficient of −0.80, indicating a moderately negative linear correlation between peak height and self-diffusion coefficient.

Table 1 also includes self-diffusion coefficients and peak heights reported by Schwegler et al.[13] for BO and CP molecular dynamics simulations using the Perdew-Burke-Ernzerhof exchange/correlation functional. Because these runs are at a different state point (slightly lower temperature

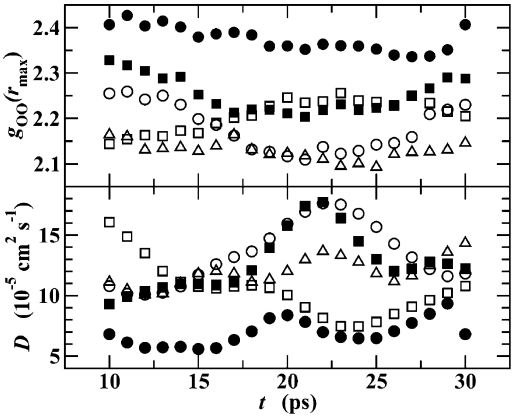

Figure 6. Evolution of the peak height of the first maximum in the oxygen−oxygen radial distribution function (top) and of the diffusion coefficient (bottom). Data points are given for the peak height and diffusion coefficient calculated over the previous 10 ps. The symbols are the same as in Figure 5.

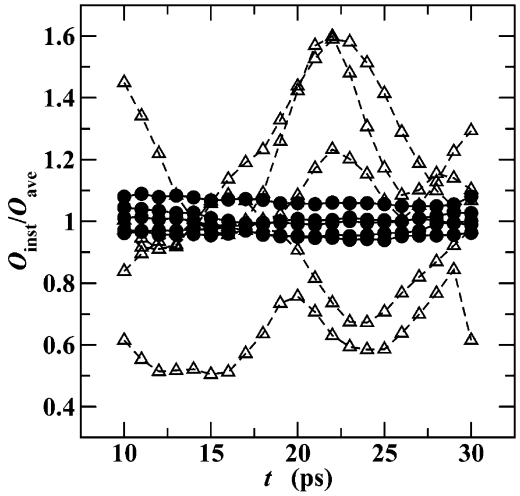

Figure 7. The ratio of the instantaneous peak height (filled circles) and self-diffusion coefficient (open triangles) to the average value across all simulations as a function of time. Data points are given for properties computed over the previous 10 ps. Lines are drawn as guides for the eye.

but significantly higher density) and use a different functional, they cannot be compared directly to the simulations performed in this work. However, an attempt can be made to explain the reported difference using insight acquired from this work. The difference in the reported height of the first peak of the oxygen−oxygen radial distribution function between CP and BO runs performed by Schwegler et al. near the same nuclear kinetic temperature (400 K) is 0.5, and the difference in self-diffusion coefficient is around a factor of 2. By using a linear-least-squares analysis and fitting a line to the data in Figure 5, one can compute the expected diffusion coefficients for a change in peak height from 2.0 to 2.5 (which includes the range of values found here and over which the data appears to be linear). This results in a change of diffusion coefficient of a factor of 3, providing evidence that the reported difference in ref 13 could be largely due to the difference in structure (peak heights of 2.6 and 3.1). Furthermore, one might expect larger statistical uncertainties for the simulations by Schwegler et al. because they were run only for 20 ps and yield substantially lower self-diffusion coefficients (presumably because of the higher density), i.e., the trajectories reached much smaller MSDs (and, hence, fewer escapes from the solvation shell) than those reported here.

Looking at the evolution of the system's properties over time is a worthwhile exercise in several respects. It can give information on the extent to which properties fluctuate and correlate. Unfortunately the self-diffusion constant (being the long-time limit of the Einstein relation) is not obtainable from an instantaneous snapshot or even a short time interval. Thus, as above, we determined this value here over the 2.0−7.0 ps range of 10 ps blocks but repeat this procedure for multiple initial times along the trajectory to follow the evolution. Figure 6 shows a plot of the first maximum in the oxygen−oxygen radial distribution function and of the self-diffusion coefficient as a function of simulation time with the former averaged over the previous 10 ps and the latter obtained from an Einstein plot of the full 10 ps. This produces data points that are necessarily correlated (each point overlaps 90% with its neighbors), but it still provides insight into the evolution of the system. It appears that for all five simulations these two properties undergo fluctuations (versus a drift that would signal poorly equilibrated samples). It is evident that the correlation times for these systems are on a scale approaching the simulation length since no system undergoes more than two complete fluctuations. The figure also depicts the same trend as is seen in Figure 5, namely that a more structured liquid-phase yields a smaller self-diffusion coefficient as well as showing significant overlap between the BO and CP simulations.

Figure 7 graphically illustrates another interesting feature of these simulations. The ratio of the 10 ps interval values in Figure 6 with the respective average value calculated from all five simulations is plotted as a function of time. These results demonstrate that the fluctuations of the self-diffusion coefficient are significantly greater than that of the first peak height of the oxygen−oxygen radial distribution function. Specifically, no value of the peak height differs from the average by more than 10%. On the other hand, some values of the instantaneous mean-square-displacement are found 50% higher or lower than the mean value. This is also demonstrated in Table 1 by the much larger confidence intervals attached to the self-diffusion coefficient. Therefore small uncertainties in the structure of a simulation can lead to even larger uncertainties in the diffusion coefficient, and one should be very cautious in comparing the transport properties of simulations with significant differences in structure. Although the magnitude of the fluctuations in the structure is small (and might therefore be overlooked), the correlation times are very long, i.e., an estimation of the statistical uncertainties from block averages needs to be viewed with caution.

It has been found that under some conditions, water described by certain density functionals may exist in a glassy state even at elevated temperatures.[33,34] Although the MSDs from this work (see Figure 4) appear to be quite linear (and there is no indication that they would reach a plateau), two tests were carried out to ensure that water under these

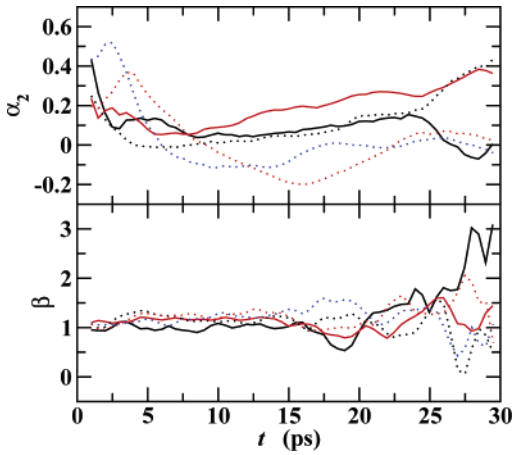

Figure 8. The values of the α_2 (top) and β (bottom) parameters as a test of glassy diffusion. The line styles and colors are the same as Figure 2.

conditions is truly in a liquid state. The first indicator, α_2, is given by

$$\alpha_2(t) = \frac{\langle |\mathbf{r}(t) - \mathbf{r}(0)|^4 \rangle}{3\langle |\mathbf{r}(t) - \mathbf{r}(0)|^2 \rangle^2} - 1 \tag{2}$$

and decays to zero for random walk statistics.[35] The second indicator of diffusive dynamics, β, is given by

$$\beta(t) = \frac{\mathrm{d}\ \ln(\langle |\mathbf{r}(t) - \mathbf{r}(0)|^2 \rangle)}{\mathrm{d}\ \ln(t)} \tag{3}$$

A value of unity for this parameter indicates that the system is diffusing in a liquid regime. Figure 8 shows plots of both these indicators over the full trajectories for all five simulations. As for the MSDs, these indicators were computed using multiple origins spaced 0.5 ps apart. Because β is a derivative, this indicator would be artificially altered close to these origins (examination of Figure 4 reveals discontinuities here). Consequently, it was decided to compute

$$\beta(t) = \frac{\ln(\langle |\mathbf{r}(t + 0.5) - \mathbf{r}(0)|^2 \rangle) - \ln(\langle |\mathbf{r}(t - 0.5) - \mathbf{r}(0)|^2 \rangle)}{\ln(t + 0.5) - \ln(t - 0.5)} \tag{4}$$

With this finite-difference method the discontinuities do not generate large jumps in β. Origins taken every 0.05 ps did not give qualitatively different results, so 0.5 ps is used here for consistency.

The indicator $\beta(t)$, as shown in Figure 8, is equal to unity for all five runs in the region of good statistics (time scales up to about 15 ps). Poor statistics after this time lead to fluctuations around unity. The plot of α_2 as a function of time is a little less clear. One expects this parameter to tend to zero at long times, if the molecular distances adopt a Gaussian distribution. For all simulations, α_2 hovers around zero for intermediate times, but then it begins to diverge again. At long times, this can be explained by poor statistics, just like for β and the MSD. For short times the configurations are still correlated, so motion is not completely random, and α_2 is not anticipated to be zero. A combination of Figures 4 and 8 leads to the conclusion that water represented by the BLYP exchange/correlation functional is not glassy at $T = 423$ K and $\rho = 0.71$ g cm^{-3}.

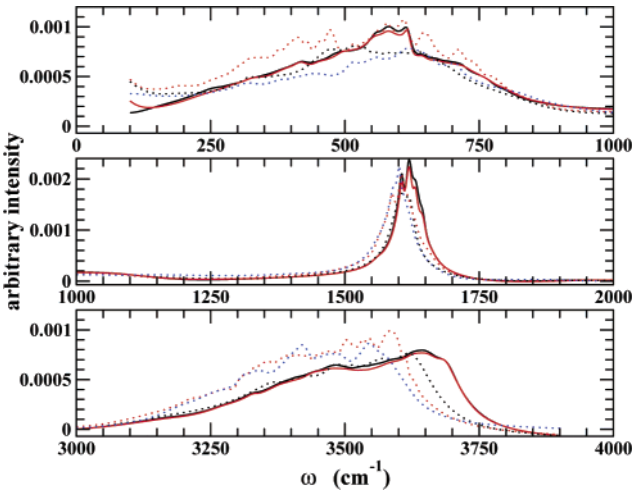

Figure 9. Power spectra computed from the regularized resolvent transform of the total velocity autocorrelation function.[36,37] The spectrum is divided into three regions (from top to bottom: librations, bending motion, and stretching modes) for clarity. The line styles and colors are the same as Figure 2.

Dynamical information of water interacting with its local environment can be gleaned from the vibrational power spectrum. It was found here that the Fourier transform (FT) of the total velocity autocorrelation function could not adequately resolve all low-frequency modes (less than 1000 cm^{-1}) of these systems. Therefore, the power spectra were generated with the regularized resolvent transform (RRT) method.[36,37] Like FT, RRT is also a direct transform of the data from the time domain into the frequency domain and is exactly equivalent to discrete FT when the frequency spectra can be represented by a sum of sinusoids. The resulting spectra are shown in the three sections of Figure 9. The regions shown correspond to the molecular librations, the H−O−H bending motion, and the O−H stretching modes. Whereas the self-diffusion coefficient shows no statistically significant fictitious mass effects, the power spectra in the mid-infrared region do show signs of dynamic retardation due to larger masses. This is in agreement with previous works[16,17,38−40] and further validates the use of a scaling parameter when analyzing the mid-infrared region to extrapolate the frequency to the limit of an infinitely small fictitious mass. The effect of the electronic mass parameter on the librational modes of water is less clear. It should also be noted that the BO trajectories appear to yield "smoother" power spectra than the CP simulations despite that an equal time span was covered in the trajectories.

The peak "position" is not well defined for the broad peaks obtained here for the librational and stretching modes (shown in the top and bottom panels of Figure 9). Consequently, Table 2 lists the median values of each peak in the RRT power spectra computed by integrating from an arbitrary intensity value (close to zero) on one side of the peak to the same value on the other side. These median peak positions show a systematic red-shift for the bending and stretching modes in the CP trajectories, with the magnitude of the shift

Table 2. Median Locations for the Three Vibrational Modes (in units of cm^{-1})

run	libration	bend	stretch
BO-1	551	1617	3522
BO-2	553	1617	3525
CP-100	498	1605	3491
CP-200	495	1599	3455
CP-300	529	1595	3446

relative to the BO value being smallest for CP-100 and largest for CP-300. The median values for the librational peak of the CP simulations show a red-shift when compared to the BO runs, but increasing the magnitude of the fictitious electronic mass does not necessarily lead to a further shift in the peak position. The evident, but not systematic, shift suggests large uncertainties in the low-frequency region of the spectra, a concern supported by the short simulation length but obfuscated by the agreement between the BO simulations (see below).

One striking feature present in both Figure 9 and Table 2 is the close agreement obtained for both BO runs. The variations between the two spectra are minimal, despite the difference in structure and diffusivity highlighted in Figures 2−4. This agreement lends credence to the belief that the differences seen in the CP simulations are not artifacts of the analysis procedure and reaffirms conclusions from earlier work that certain properties (in particular, those directly related to forces and momentum via changes of the mass) are influenced by the use of the CP method.[16,17,27]

Finally, one should note that the librational part of the spectrum observed here does not show the distinct features observed in CP molecular dynamics simulations for the water spectrum at ambient conditions.[41] The most likely explanation is that the tetrahedral hydrogen-bonded network is very fluctuational at the high-temperature, low-density conditions investigated here. Thus, interchange between different local configurations is fast, and their lifetimes are too short to establish specific librational features. This explanation is supported by recent experimental analysis of vibrational lifetimes in liquid water.[42]

Conclusions

A series of long molecular dynamics trajectories for liquid water near 423 K obtained from BO molecular dynamics and CP molecular dynamics with varying values of the fictitious mass parameters, μ, has allowed us to look at the structural and transport properties of water using density functional theory with BLYP exchange and correlation. All five simulations show similar structural properties with a range in the height of the first peak in the oxygen−oxygen radial distribution function of about 0.2. It has been concluded before,[12,14] and shall be reiterated here, that reasonable values of μ (in other words, values that do not lead to a large drift in the electronic kinetic energy and a subsequent lowering of ionic temperature) do not produce statistically significant differences in structural properties on the observed simulation time scales.

All five simulations show large fluctuations and hence large uncertainties for the self-diffusion coefficient. Again, on the simulation time scales used here there does not appear to be a statistically significant difference in transport properties between BO and CP molecular dynamics simulations as long as reasonable values of μ are used. If one assumes that the statistical uncertainties for the self-diffusion coefficient are solely a function of the distance a molecule travels on average, simulations near ambient temperature and density would require around 500 ps to obtain a diffusion coefficient with the same statistical uncertainty (about 50%) as found in this work. Consequently, it appears that only order of magnitude estimates for transport properties are reliable using current technology and algorithms for first principles simulations at ambient conditions (with the use of higher temperatures and lower densities enabling somewhat more precise values).

From this it can be concluded that, for reasonable values of the fictitious mass parameter, several physical properties (including structural information and the self-diffusion coefficient) of CP and BO simulations are indistinguishable on time scales of tens of picoseconds. However, it should be emphasized that even the CP trajectories with $\mu = 100$ or 200 au show a small increase of the fictitious electronic energy over the 30 ps trajectory. Thus, for these fictitious mass parameters there will be a much longer time scale over which this increase will lead to a noticeable decrease of the ionic temperature.

One observable that is clearly influenced by the choice of μ is the power spectrum, in which using CP dynamics with fictitious electronic mass shifts the spectrum into regions of lower frequency, even for small values of this parameter. A likely explanation for the manifestation of fictitious mass effects in the power spectrum is that this observable is governed directly by the instantaneous forces and the reduced mass of a given normal mode. References 16, 17, and 27 point out that the instantaneous forces of CP simulations with any value of the electronic mass are different than the BO forces for an identical system. On the other hand, properties that depend on free energies (e.g. the radial distribution function) or are governed by long-time processes involving free energy barriers (e.g., diffusive transport) should be significantly less affected given a reasonable choice of μ because instantaneous differences in the forces can cancel upon averaging.

Acknowledgment. We thank Juerg Hutter and Ed Maginn for many helpful discussions and Larry Fried and Charlie Westbrook for their ongoing support of this work. Financial support from the National Science Foundation Grants CTS-0138393 and ITR-0428774, a 3M Foundation Graduate Fellowship (M.J.M.), and a Department of Energy Computational Science Graduate Fellowship (M.J.M.) are gratefully acknowledged. Part of this work was performed under the auspices of the U.S. Department of Energy by the University of California Lawrence Livermore National Laboratory (LLNL) under contract No. W-7405-Eng-48. J.I.S. and M.J.M. thank the University Relations Program (LLNL) for hosting their sabbatical visit. Computer resources were provided by LLNL Computing and the Minnesota Supercomputing Institute.

References

(1) Hansen, J. P.; McDonald, I. R. *Theory of Simple Liquids*, 2nd ed.; Academic Press: New York, NY, 1986.

(2) Allen, M. P.; Tildesley, D. J. *Computer simulation of liquids*; Oxford University Press: Oxford, England, 1987.

(3) Barker, J. P.; Watts, R. O. *Chem. Phys. Lett.* **1969**, *3*, 144.

(4) Car, R.; Parrinello, M. *Phys. Rev. Lett.* **1985**, *55*, 2471.

(5) Laasonen, K.; Sprik, M.; Parrinello, M.; Car, R. *J. Chem. Phys.* **1993**, *99*, 9080.

(6) Marx, D.; Tuckerman, M. E.; Hutter, J.; Parrinello, M. *Nature* **1999**, *397*, 601.

(7) Cavazzoni, C.; Chiarotti, G. L.; Scandolo, S.; Tosatti, E.; Bernasconi, M.; Parrinello, M. *Science* **1999**, *283*, 44.

(8) Geissler, P. L.; Dellago, C.; Chandler, D.; Hutter, J.; Parrinello, M. *Science* **2001**, *291*, 2121.

(9) Kuo, I.-F. W.; Mundy, C. J. *Science* **2004**, *303*, 658.

(10) Tateyama, Y.; Blumberger, J.; Sprik, M.; Tavernelli, I. *J. Chem. Phys.* **2005**, *122*, 234505.

(11) Asthagiri, D.; Pratt, L. R.; Kress, J. D. *Phys. Rev. E* **2003**, *68*, 041505.

(12) Grossman, J. C.; Schwegler, E.; Draeger, E. W.; Gygi, F.; Galli, G. *J. Chem. Phys.* **2004**, *120*, 300.

(13) Schwegler, E.; Grossman, J. C.; Gygi, F.; Galli, G. *J. Chem. Phys.* **2004**, *121*, 5400.

(14) Kuo, I.-F. W.; Mundy, C. J.; McGrath, M. J.; Siepmann, J. I.; VandeVondele, J.; Sprik, M.; Hutter, J.; Chen, B.; Klein, M. L.; Mohamed, F.; Krack, M.; Parrinello, M. *J. Phys. Chem. B* **2004**, *108*, 12990.

(15) McGrath, M. J.; Siepmann, J. I.; Kuo, I.-F. W.; Mundy, C. J.; VandeVondele, J.; Hutter, J.; Mohamed, F.; Krack, M. *ChemPhysChem* **2005**, *6*, 1894.

(16) Tangney, P.; Scandolo, S. *J. Chem. Phys.* **2002**, *116*, 14.

(17) Tangney, P. *J. Chem. Phys.* **2006**, *124*, 044111.

(18) McGrath, M. J.; Siepmann, J. I.; Kuo, I.-F. W.; Mundy, C. J.; VandeVondele, J.; Mohamed, F.; Krack, M. *J. Phys. Chem. A* **2006**, *110*, 640.

(19) Becke, A. D. *Phys. Rev. A* **1988**, *38*, 3098.

(20) Lee, C.; Yang, W.; Parr, R. G. *Phys. Rev. B* **1988**, *37*, 785.

(21) CPMD, Version 3.9.2, Copyright IBM Corp. 1990−2001, Copyright MPI für Festkörperforschung. Stuttgart 1997−2005. http://www.cpmd.org.

(22) Kohn, W.; Sham, L. A. *Phys. Rev. A* **1965**, *140*, A1133.

(23) Troullier, N.; Martins, J. L. *Phys. Rev. B* **1991**, *43*, 1993.

(24) Kleinman, L.; Bylander, D. M. *Phys. Rev. Lett.* **1982**, *48*, 1425.

(25) Silvestrelli, P. L. *Phys. Rev. B* **1999**, *59*, 9703.

(26) Chen, B.; Ivanov, I.; Park, J. M.; Parrinello, M.; Klein, M. L. *J. Phys. Chem. B* **2002**, *106*, 12006.

(27) Pastore, G.; Smargiassi, E.; Buda, F. *Phys. Rev. A* **1991**, *44*, 6334.

(28) Mantz, Y. A.; Chen, B.; Martyna, G. J. *Chem. Phys. Lett.* **2005**, *405*, 294.

(29) Tassaing, T.; Bellissent-Funel, M.-C.; Guillot, B.; Guissani, Y. *Europhys. Lett.* **1998**, *42*, 265.

(30) Boero, M.; Terakura, K.; Ikeshoji, T.; Liew, C. C.; Parrinello, M. *J. Chem. Phys.* **2001**, *115*, 2219.

(31) Lamb, W. J.; Hoffman, G. A.; Jonas, J. *J. Chem. Phys.* **1981**, *74*, 6875.

(32) Mills, R. *J. Phys. Chem.* **1973**, *77*, 685.

(33) Sit, P. H.-L.; Marzari, M. *J. Chem. Phys.* **2005**, *122*, 204510.

(34) VandeVondele, J.; Mohamed, F.; Krack, M.; Hutter, J.; Sprik, M.; Parrinello, M. *J. Chem. Phys.* **2005**, *122*, 014515.

(35) McQuarrie, D. A. *Statistical Mechanics*; Harper and Row: New York, 1976.

(36) Mandelshtam, V. A. *Prog. Nucl. Magn. Reson. Spectrosc.* **2001**, *38*, 159.

(37) Chen, J. H.; Shaka, A. J.; Mandelshtam, V. A. *J. Magn. Reson.* **2000**, *147*, 129.

(38) Tobias, D. J.; Jungwirth, P.; Parrinello, M. *J. Chem. Phys.* **2001**, *114*, 7036.

(39) Kuo, I.-F. W.; Tobias, D. J. *J. Phys. Chem. A* **2002**, *106*, 10969.

(40) Goncharov, A. F.; Goldman, N.; Fried, L. E.; Crowhurst, J. C.; Kuo, I.-F. W.; Mundy, C. J.; Zaug, J. M. *Phys. Rev. Lett.* **2005**, *94*, 125508.

(41) Silvestrelli, P. L.; Bernasconi, M.; Parrinello, M. *Chem. Phys. Lett.* **1997**, *277*, 478.

(42) Eaves, J. D.; Loparo, J. J.; Fecko, C. J.; Roberts, S. T.; Tokmakoff, A.; Geissler, P. L. *Proc. Natl. Acad. Sci.* **2005**, *102*, 13019.

CT6001913